Mechanism of length-induced magnetism in polyacene molecules

Yuanyuan Miao,[1] Liyuan Chen,[1] Guangping Zhang,[1] Chuankui Wang,[1] Junfeng Ren,[1,*] Carsten Timm,[2,3,†] and Guichao Hu[1,‡]

[1]*School of Physics and Electronics, Shandong Normal University, Jinan 250100, China*
[2]*Institute of Theoretical Physics, Technische Universität Dresden, 01062 Dresden, Germany*
[3]*Würzburg-Dresden Cluster of Excellence ct.qmat, Technische Universität Dresden, 01062 Dresden, Germany*

(Received 23 December 2021; revised 2 March 2022; accepted 3 March 2022; published 14 March 2022)

Within the celebrated Su-Schrieffer-Heeger model including electron-lattice and electron-electron interactions, the electronic ground state of polyacene (n-acene) is studied as a function of molecular length n. The results demonstrate that the ground state exhibits a phase transition from a nonmagnetic state to an antiferromagnetic state at a critical length of $n = 7$. The magnetism is explained by calculating the lattice distortion and the related average hopping rate of the π electrons. It is revealed that in polyacenes, there exist two competing mechanisms that minimize the molecular energy, namely the lattice dimerization and the formation of an antiferromagnetic spin density. Since the dimerization is restricted to the regions near the ends of the molecules the former mechanism is dominant for short molecules, which therefore assume a nonmagnetic state. When the length is increased beyond the critical value, the lattice dimerization in the middle of the molecule is reduced and a rapid drop of the average hopping rate occurs. This makes the second mechanism dominant and the associated antiferromagnetic state is stabilized. The effect of different interaction strengths and values of hopping integrals on the critical length is discussed. The results are confirmed by first-principles calculations. Suggestions for the design of organic antiferromagnets with a similar ladder structure are also given.

DOI: 10.1103/PhysRevB.105.094419

I. INTRODUCTION

Organic spintronics is an emerging field that explores the magnetism and spin-dependent transport properties in organic materials and designs functional organic spintronic devices such as spin valves, spin filters, and spin diodes [1–6]. The field is stimulated by the merits of organic materials in spintronics, which include the prospect of low-cost and flexible devices, long spin relaxation times [7], and a huge number of candidate molecules. A key issue is the realization of magnetism in organics. Due to the absence of d electrons, most organic molecules are nonmagnetic (NM). In previous studies, the magnetism in organics has usually been achieved by spin injection from ferromagnetic (FM) metals [8], by designing magnetic molecules containing transition-metal ions [9], or by using spin radicals [10,11]. The realization of intrinsic magnetism in organics requires the search for novel materials.

Polyacenes are polyaromatic hydrocarbons consisting of linearly fused benzene rings, where the structure can be viewed as two cross-linked chains of polyacetylene. Over the past few decades, as typical organic π-conjugated materials, polyacenes have been widely applied in organic luminescence [12–14] and molecular electronics [15–19]. In experiments, the synthesis of long polyacenes is challenging due to their decreasing stability for increasing length [20–30]. Up to now, the longest molecule is dodecacene with 12 rings ($n = 12$), which has been synthesized by Eisenhut *et al.* [31]. An interesting phenomenon indicated by several experimental works is that polyacene shows length-dependent magnetism. Short polyacenes such as tetracene ($n = 4$) and pentacene ($n = 5$) are NM molecules [32,33]. In 2010, Tönshoff *et al.* [25] pointed out that the ground state of nonacene ($n = 9$) has an antiferromagnetic (AFM) ground state.

This length-induced magnetism has triggered considerable interest in theoretical studies. For example, by using an unrestricted B3LYP hybrid density functional method with the 6-31G* basis in Gaussian98, Bendikov *et al.* [34] have found that the polyacene molecules for $n > 6$ become disjoint diradicals with two unpaired electrons, which form a spin singlet with AFM order. Jiang *et al.* [35] have studied the electronic state of longer polyacene molecules (n up to 40) using density functional theory (DFT) in the Vienna *ab initio* simulation package (VASP). By calculating the total energy and spin density, they have obtained a stable AFM state for $n > 7$ and found that the AFM state is not a diradical but rather the number of unpaired electrons increases with the size of the polyacene. The length-induced AFM ground state is also confirmed by other first-principles calculations with different hybrid functionals [32,36], where the critical length is around $n = 7$ or 8. Several first-principles calculations even suggested that the ground state can be a triplet above a critical length [37,38]. First-principles calculations confirmed the existence of length-induced magnetism in polyacene, although the understanding of the intrinsic mechanism is still inadequate. Model calculations including density

*Corresponding author: renjf@sdnu.edu.cn
†Corresponding author: carsten.timm@tu-dresden.de
‡Corresponding author: hgc@sdnu.edu.cn

matrix renormalization group (DMRG) [39,40] and tight-binding methods [41,42] have also been performed for infinite polyacene or similar cross-linked ladders, where an AFM ground state is predicted and the roles of electron-phonon coupling and electronic correlations are discussed. These calculations are helpful to understand the magnetism of the polyacene in the limit of long chains, which make the direct comparison with graphene nanoribbon feasible, while the details around the critical length are seldom discussed. The length effect on spin-dependent transport in polyacene-based junctions has also been studied in recent years [32,43–46].

The above research shows the diversity of magnetism in polyacenes. Although the magnetism in finite polyacenes has been confirmed by first-principles calculations, the physical mechanism has not been discussed much and remains obscure. Model calculations, usually for periodic systems, have clarified the picture in the limit of long chains, which is, however, of limited relevance for the understanding of real molecules with $n \leqslant 12$, especially of the mechanism around the critical value where the structural deformation and the size effect are important. In this paper, we adopt the celebrated Su-Schrieffer-Heeger (SSH) model [47] to investigate the ground-state properties of polyacene molecules of various lengths. The SSH model contains electron-lattice (*e-l*) coupling in polymers, can thus describe the bond distortion, and is widely used and successful in understanding the electric and magnetic properties of polymers. In this paper, the mechanism of length-induced magnetism is analyzed by investigating the electronic states and lattice structure in the presence of *e-l* coupling and size effect.

The remainder of this paper is organized as follows. In Sec. II, we introduce the model Hamiltonian for the polyacene molecules and the details of the theoretical method. The results of the numerical calculations are presented and analyzed in Sec. III, where the mechanism of the magnetic transition is discussed and the consequences of changing model parameters are studied. A brief summary is given in Sec. IV.

II. MODEL AND METHOD

The model structure of our calculated polyacene molecules is shown in Fig. 1. The molecule is described by an extended SSH model including *e-l* coupling, on-site electron-electron (*e-e*) interaction, and interchain coupling. The Hamiltonian of the molecule is written as

$$H = \sum_j H_j + H_c. \tag{1}$$

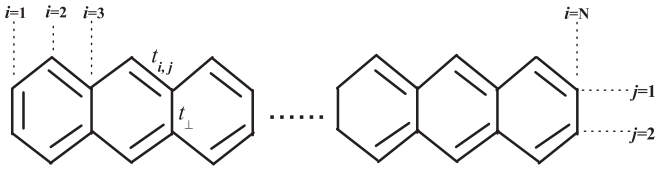

FIG. 1. Simplified structure of polyacene molecules.

Here, H_j is the Hamiltonian of a single chain with

$$H_j = -\sum_{i,\sigma} t_{i,j}\left(c^\dagger_{i+1,j,\sigma}c_{i,j,\sigma} + \text{H.c.}\right) + \frac{1}{2}K\sum_i y^2_{i,j} + U\sum_i c^\dagger_{i,j,\uparrow}c_{i,j,\uparrow}c^\dagger_{i,j,\downarrow}c_{i,j,\downarrow}, \tag{2}$$

where $t_{i,j} = t_0 - \alpha y_{i,j}$ is the hopping integral of the π electrons along the jth chain ($j = 1, 2$), α is the *e-l* coupling constant, $y_{i,j}$ is the lattice distortion with $y_{i,j} = u_{i+1,j} - u_{i,j}$, $u_{i,j}$ is the lattice displacement of the carbon atom at the ith site of the jth chain, and $c^\dagger_{i,j,\sigma}(c_{i,j,\sigma})$ denotes the creation (annihilation) operator of an electron at the ith site of the jth chain with spin σ. The second term is the lattice distortion energy with elastic coefficient K. The last term is the on-site *e-e* interaction between the π electrons described by the Hubbard interaction strength U. H_c is the Hamiltonian of the interchain hopping of the π electrons,

$$H_c = -\sum_{i,\sigma}^{N} t_1\delta_{i,\text{odd}}(c^\dagger_{i,1,\sigma}c_{i,2,\sigma} + \text{H.c.}), \tag{3}$$

where t_1 is the interchain hopping integral, $\delta_{i,\text{odd}}$ signifies that the interchain hopping only occurs at the odd sites of the chain with $\delta_{i,\text{odd}} = 1$ ($\delta_{i,\text{odd}} = 0$) for odd (even) atoms, and N is the total number of sites in a single chain.

With the mean-field (Hartree) approximation to treat the *e-e* interaction, which has been used in previous calculations for polyacene and other conjugated polymers [42,48–50], the electronic states can be obtained by solving the eigenequations of the system,

$$\varepsilon_{\mu,\sigma}Z^\sigma_{\mu,i,j} = -t_{i,j}Z^\sigma_{\mu,i+1,j} - t_{i-1,j}Z^\sigma_{\mu,i-1,j} + U\bar{n}_{i,-\sigma,j}Z^\sigma_{\mu,i,j} - t_1\delta_{i,\text{odd}}Z^\sigma_{\mu,i,j\pm1}. \tag{4}$$

Here, $\varepsilon_{\mu,\sigma}$ is the eigenvalue and $Z^\sigma_{\mu,i,j}$ is the eigenfunction in Wannier space. $\bar{n}_{i,\sigma,j}$ is the average electron number on the ith site of the jth chain with spin σ,

$$\bar{n}_{i,\sigma,j} = \sum_{\mu,\text{occ.}} \left|Z^\sigma_{\mu,i,j}\right|^2, \tag{5}$$

where occ. means that the sum is over all occupied states.

The eigenequations are solved with the initial lattice configuration $y_{i,j}$ and electron density $\bar{n}_{i,\sigma,j}$. After obtaining the eigenfunctions $Z^\sigma_{\mu,i,j}$, the new lattice configuration is calculated as

$$y_{i,j} = -\frac{2\alpha}{K}\sum_{\mu,\sigma,\text{occ}} Z^\sigma_{\mu,i,j}Z^\sigma_{\mu,i+1,j} + \frac{2\alpha}{(N-1)K}\sum_i\sum_{\mu,\sigma,\text{occ}} Z^\sigma_{\mu,i,j}Z^\sigma_{\mu,i+1,j}. \tag{6}$$

Here, fixed-end boundary conditions are adopted with $u_{1,j} = u_{N,j} = 0$, which guarantees the molecular chain length to be unchanged during structural relaxation. It has been checked that the boundary condition is not crucial for the molecular magnetism. The electron number is also recalculated using Eq. (5). Eqs. (4)–(6) need to be solved iteratively, until a self-consistent solution is reached. In each iteration, the energy levels are reordered and the states of lowest energy

are occupied by the given number of electrons. After the iteration, the spin density $\rho_{s,i,j}$ can be obtained as $\rho_{s,i,j} = \frac{1}{2}(\bar{n}_{i,j,\uparrow} - \bar{n}_{i,j,\downarrow})$ in units of $\hbar$.

For the numerical calculations, we take the parameters in each chain as those of polyacetylene due to the similar structure [3,10,11]: $t_0 = 2.5\,\text{eV}$, $\alpha = 4.1\,\text{eV/Å}$, and $K = 21.0\,\text{eV/Å}^2$, which have been frequently used for other typical conjugated polymers. The interchain hopping integral and *e-e* interaction are expressed by dimensionless parameters with $t_\perp = t_1/t_0$ and $u = U/t_0$. We take the value of $t_\perp = 1.0$ for polyacene, since first-principles and related calculations [34,35,40] show that the interchain bond lengths are close to intrachain bonds. Although slight changes of intrachain bond length at the two ends are also mentioned, the amplitude is much smaller than the intrachain bond length. For simplicity, a uniform $t_\perp$ is used. $u = 1.5$ is used for the *e-e* interaction, which generates a ground-state band gap of about 1.0 eV for long polyacenes close to other first-principles and experimental works [31,51,52]. The effect of the strength of $t_\perp$ and u will also be further studied in our calculations.

III. RESULTS AND DISCUSSION

A. NM-AFM transition in finite polyacenes

To determine the ground state of polyacene, we first calculate the total energy of polyacene with $n = 4$–11 in the AFM and FM states relative to the NM state. To that end, we start iterations in three different initial spin states, namely the NM, AFM, and FM states, which are achieved by setting the initial spin density at each site to zero, antiferromagnetic and ferromagnetic, respectively. The initial lattice configuration of each chain is a dimerization with $y_{i,j} = 0.08 \times (-1)^i$. The calculation precision is 10^{-8} for $|\Delta y_{i,j}|$ between two iterations. Since the iterative calculation cannot break symmetries that are present in the initial state, a NM initial state remains NM, whereas the AFM and FM initial states can evolve into the NM state if they are unstable. As shown in Fig. 2, the NM phase is the ground state when n is smaller than 7. For $n \geqslant 7$, the AFM state becomes the lowest-energy state. For $n \geqslant 10$, the FM state appears as a metastable state, which is lower than the NM state but higher than the AFM state. The critical length of $n = 7$ for the NM-AFM phase transition is consistent with previous first-principles reports [34,35,43].

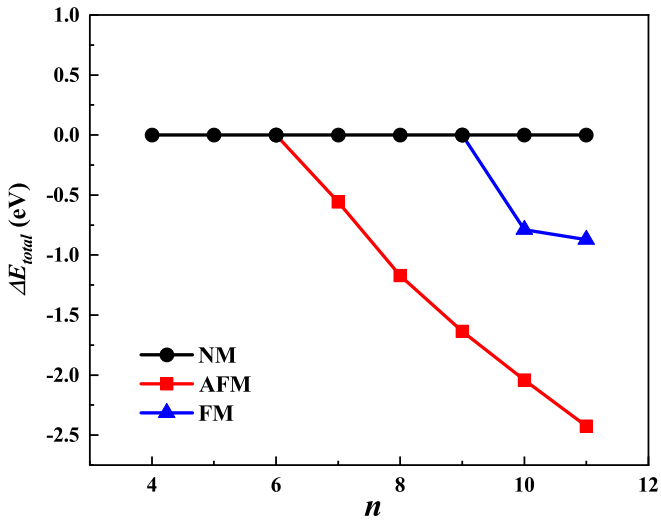

FIG. 2. Relative total energy $\Delta E_{\text{total}} = E_{ms} - E_{\text{NM}}$ of the molecule as a function of length. *ms* can be taken as NM, AFM, and FM states, respectively.

The NM-AFM phase transition can be confirmed by investigating the spin density along the molecular chains. We have checked the spin density for the ground state from $n = 5$ to $n = 8$. As shown in Figs. 3(a) and 3(b), the spin density for $n = 5$ and 6 is zero within numerical precision, which indicates a NM state. For $n = 7$ and 8, an obvious AFM spin density wave appears, as shown in Figs. 3(c) and 3(d). The amplitude of the spin density in the middle of the chain is larger than near the ends. The spin density in the two chains is opposite and is larger at the even-numbered sites, i.e., the sites without cross-linking bonds. To get a quantitative view of the length-induced magnetism, we have calculated the total spin in a single chain, $M_j = |\sum_i \rho_{s,i,j}|$, and the average spin on one chain per ring, $m_j = M_j/n$. As shown in Fig. 4, the total spin remains zero for $n \leqslant 6$ and jumps to 0.25 for $n = 7$. The average spin on one chain per ring is 0.035 for $n = 7$. The two quantities increase nonlinearly with length and reach 0.64 and 0.059, respectively, at $n = 11$.

To give a deeper insight into the phase transition of the ground state, the probability distribution of the highest occupied molecular orbital (HOMO) for $n = 6$ and $n = 7$ is depicted in Fig. 5. We find that the probability distribution at $n = 6$ is identical for spin-up and spin-down electrons on the two chains. In the case of $n = 7$, obvious spin nondegeneracy occurs for the probability distribution, where the spin-up state has higher weight on the lower chain ($j = 2$) and the spin-down state on the upper chain ($j = 1$). The probability distribution of the HOMO on each chain is close to the spin density shown in Fig. 3(c), which indicates that the spin density is mainly contributed by the HOMO. The probability distribution of other occupied orbitals has also been examined, where the spin nondegeneracy is small and is not shown here.

To understand the mechanism of the NM-AFM transition, we focus on the lattice distortion in the calculated systems since the bond length is believed to be important based on previous first-principles studies [35,39,40]. In Fig. 6, we show the lattice distortion around the critical length from $n = 5$ to 8. The lattice distortion along the upper chain is displayed (it is the same in the lower chain), while the cross-linking bonds between the two chains are assumed to be unchanged in our calculations. There is a tendency to form alternatingly short and long bonds, which is due to Peierls dimerization in the one-dimensional chains. One can clearly see a large negative distortion (i.e., shorter bonds, with larger double-bond character) for the ultimate bonds of the chains. For $n = 5$ and 6, a solitonlike lattice distortion exists in the chain where the distortion in the middle of the chain is tiny. Other polyacene molecules with smaller lengths have also been checked, with analogous results. The solitonlike distortion is caused by the odd number of sites and thus even number of bonds in each chain, which frustrates the Peierls dimerization. Such a distortion in polyacene was also reported in earlier work [40]. However, when the length reaches $n = 7$, it is found that the solitonlike distortion is destroyed and the central four bonds

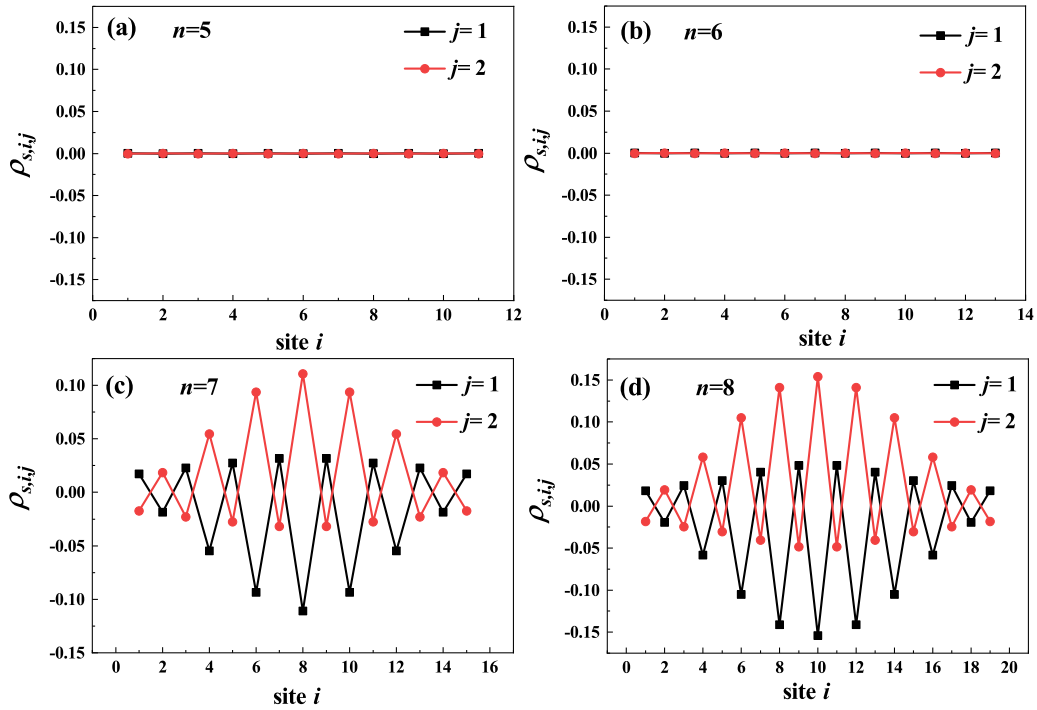

FIG. 3. Spin density on the upper and lower chains from $n = 5$ to $n = 8$ in the ground state.

are almost uniform with much smaller distortion. At $n = 8$, the dimerization of more bonds in the inner rings is reduced and the distortions seem to become incommensurate. With further increase of the length, more and more bonds in the middle of the chain tend to be nearly undistorted, while two solitonlike features remain near the two ends, as shown in Figs. 6(e) and 6(f).

The simultaneous NM-AFM transition and change of the lattice configuration indicates the vital role of the lattice deformation in the emergence of molecular magnetism. In the present model, the lattice distortion is related to the electron hopping $t_{i,j} = t_0 - \alpha y_{i,j}$. Generally, the electron hopping and the on-site e-e interaction are competing in the generation of magnetism [53,54]. Strong Hubbard repulsion favors magnetic order since the unequal occupation of spin-up and spin-down orbitals partly avoids the repulsion. On the other hand, larger hopping amplitudes reduce the electronic density of states, which makes the Hubbard repulsion less effective. This is essentially the Stoner mechanism. It here favors an AFM spin density wave with a wavelength of two nearest-neighbor bonds since the model is bipartite and half filled [55,56]. To achieve a deeper understanding, we calculate the average hopping rate $T_n = \frac{1}{2n}\sum_i t_{i,1}^2 + t_{i-1,1}^2$ of the π electrons along a chain. The results are shown in Fig. 7. One can see that the average hopping rate decreases monotonically with increasing length n. Moreover, a large drop occurs for $n = 7$, where the NM-AFM transition happens. A clearer illustration of the change of the average hopping rate between consecutive values of n is given in the inset, where ΔT_n is defined as $\Delta T_n = T_n - T_{n-1}$. Obviously, the maximum difference occurs at the critical length $n = 7$.

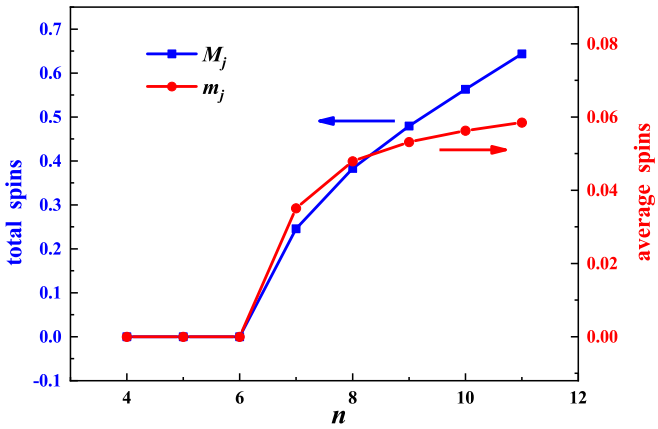

FIG. 4. Total spin on one chain (M_j) and average spin per ring (m_j) on one chain as functions of length.

Based on the previous calculations, the length-induced transition of the molecular magnetism can now be understood. For short molecules ($n < 7$), the lattice distortion plays a decisive role. The large distortion makes the average electron hopping rate relatively large, which disfavors magnetic order and the molecule takes on a NM state. With the increase of the number of rings, the distortion remains localized at the ends of the molecule and the average electronic hopping rate decreases. On the other hand, the average e-e interaction energy remains constant in the NM state since the occupation probability of each relevant Wannier orbital is fixed to 1/2. Thus, the decrease of the average hopping rate with length will finally lead to an AFM state at a specific critical length. At $n = 7$, the abrupt drop of the average hopping rate, caused by the reduction of dimerization in the middle rings, makes the e-e interaction dominant and an AFM state emerges. The continuing decrease of the average hopping rate with length suggests that the molecule will stay in the AFM ground state.

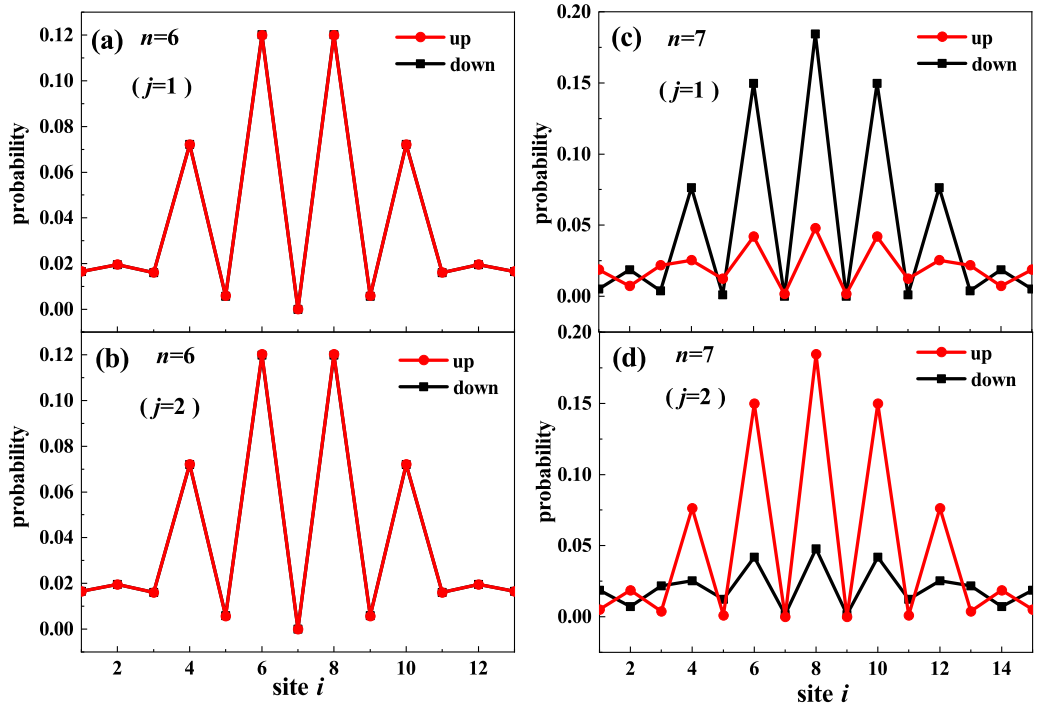

FIG. 5. Probability density of the spin-up and spin-down HOMOs in the ground state for $n = 6$ and 7.

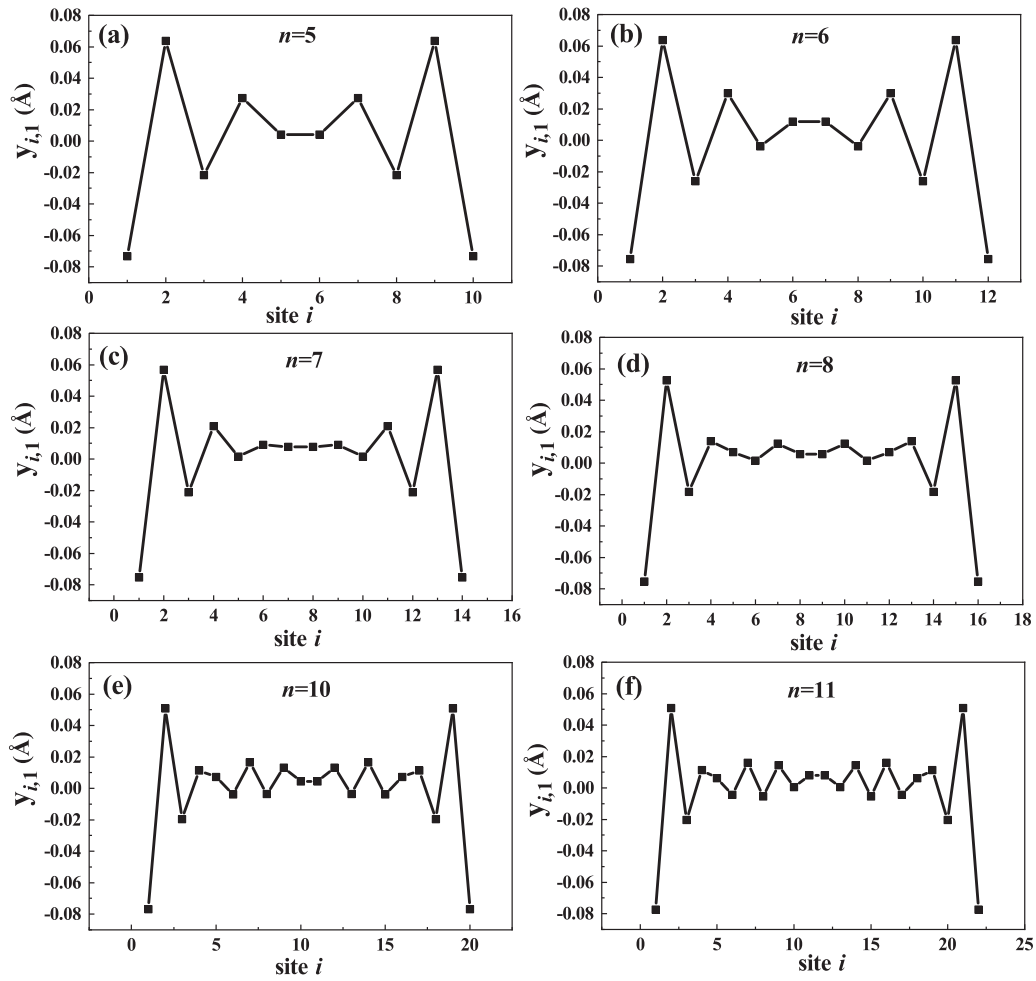

FIG. 6. Lattice distortion from $n = 5$ to $n = 11$ in the ground state.

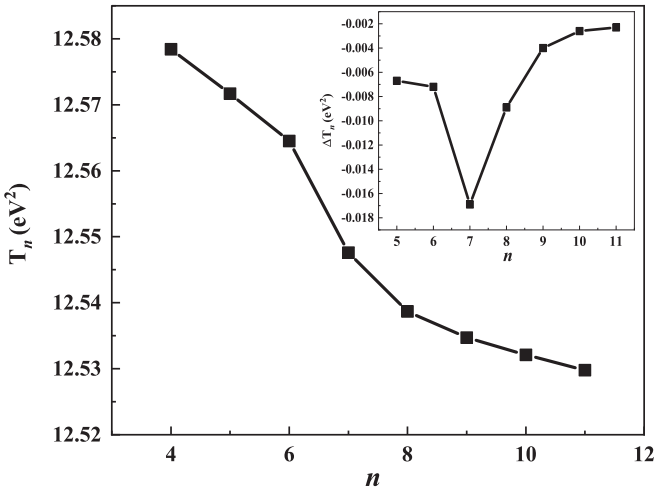

FIG. 7. Average hopping rate T_n along one chain with n from 4 to 11. The inset shows the difference $\Delta T_n = T_n - T_{n-1}$.

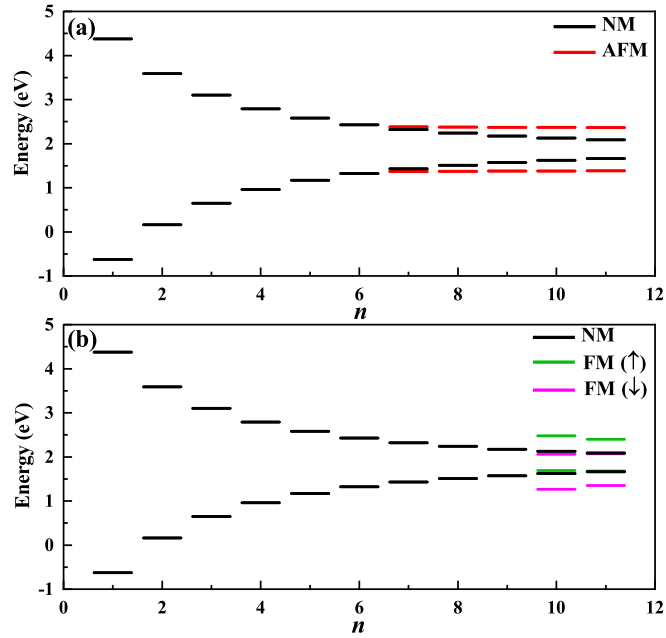

FIG. 8. Energy gap of the molecule as a function of length for the NM, AFM, and FM states.

The decrease of dimerization with length is best understood as a finite-length effect. Infinite polyacene shows relatively weak dimerization, which is controlled by the competition between the *e-e* and *e-l* interactions. As discussed above, the former favors a uniform lattice and an AFM state, while the latter favors a dimerized lattice and a NM state. For finite molecules, the dimerization is enhanced close to the ends. This is easy to understand: The presence of the ends breaks the degeneracy between the two possible dimer coverings by favoring a dimer at the ultimate two sites and disfavoring an unpaired site at the end. The increase of the chain length drives the ends apart, and thus the dimerization in the middle of the chain decreases.

The NM-AFM transition can also be understood from the molecular total energy. It is known that the dimerization minimizes the molecular total energy via reducing the electronic energy by opening a Peierls gap, while the elastic potential energy is increased [47]. The NM-AFM transition occurs together with a suppression of the lattice dimerization and hence the electronic energy should increase due to the reduction of the Peierls gap. However, the appearance of the AFM state lowers the Coulomb energy of the electrons and opens a new (Stoner) gap. This gap shows only weak length dependence since it is due to magnetic ordering, which is dominated by the bulk of the molecule, see Figs. 3 and 5. In Fig. 8, the energy gap of the molecule is illustrated by the eigenenergies of the lowest unoccupied molecular orbital (LUMO) and the HOMO as functions of the length for the NM, AFM, and FM states. It is found that the energy gap continuously decreases with increasing length for the NM state. For $n \geqslant 7$, the ground state is AFM and the energy gap remains almost unchanged, which is consistent with our analysis. In contrast, for the NM and FM states, the energy gap keeps decreasing with length, and so leads to higher electronic energy compared to the AFM state.

Note that here the dimerization of the lattice is essential for the NM-AFM transition. In the absence of dimerization ($\alpha = 0$), the NM state does not appear and the ground state is AFM state even for short lengths. As shown in Fig. 9(a), obvious AFM spin density emerges in a uniform lattice ($\alpha = 0$) at $n = 4$, while the ground state is NM for $\alpha = 4.1\,\mathrm{eV/\AA}$.

We further present the critical length for different strengths of the *e-l* interaction α in Fig. 9(b), where the hopping integral $t_\perp$ and the *e-e* interaction u are fixed. An increase of the critical length from 6 to 11 is observed when α is increased from 3.0 to 5.0 eV/Å. Obviously, a larger *e-l* coupling α suppresses the AFM order. This is because the dimerization in each chain is enhanced by α. The corresponding increase of the average hopping rate T_n favors the NM state, as we have seen.

In the present model, the interchain electron hopping integral $t_\perp$ and the *e-e* interaction u are also key parameters. In the following, we discuss the effects of the values of these two parameters on the critical length. In Fig. 10(a), we fix the *e-e* interaction u and the *e-l* coupling constant α and change the strength of the hopping term $t_\perp$. It is found that as $t_\perp$ increases from 0.5 to 1.5, the critical length n_c decreases from 16 to 4. When $t_\perp$ is less than 0.5, the NM-AFM transition is not observed in the range of our calculation ($n \leqslant 40$). The results mean that a larger $t_\perp$ favors the transition to AFM order in a finite chain. This effect can be understood from the hybridization between the two chains. For small $t_\perp$, the lattice dimerization in each chain is obvious. So, the average hopping rate T_n is relatively large. As $t_\perp$ increases, we find that the lattice dimerization and thus the average hopping rate T_n in each chain are reduced. The reduction of the dimerization induced by the increase of $t_\perp$ has been demonstrated numerically in several previous works [57,58]. The intrinsic physics can be understood as follows. With the increase of $t_\perp$, the hybridization between the states of the two chains becomes stronger, which decreases the Peierls gap and increases the electronic energy near the Fermi level. Such a change counteracts the dimerization effect, where the electron energy near the Fermi level is lowered by the Peierls gap. So, the dimerization

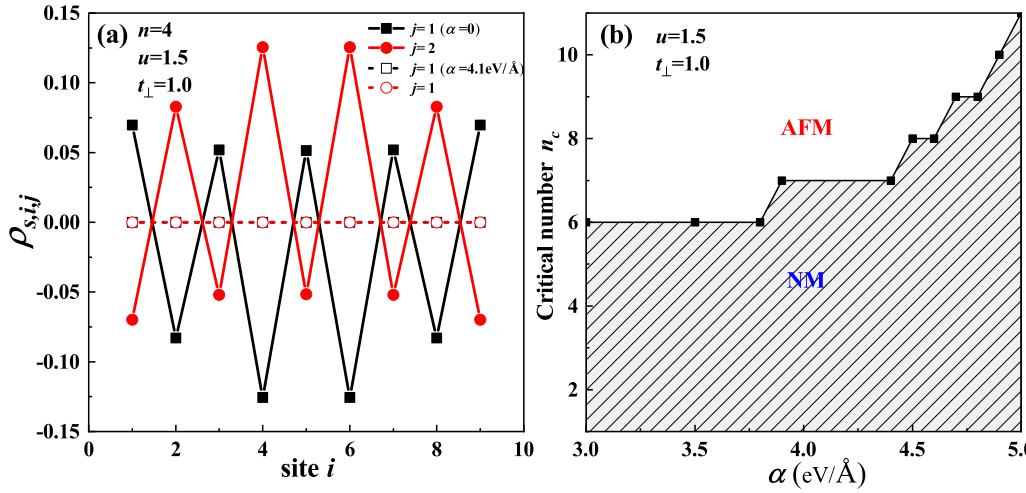

FIG. 9. (a) Spin density in one chain for $n = 4$ with and without e-l coupling α. (b) Critical length n_c of the NM-AFM transition as a function of α.

is weakened. According to the previous discussion, in this situation, AFM order is favored.

The effect of the e-e interaction u is shown in Fig. 10(b), where the interchain hopping integral $t_\perp$ and the e-l coupling constant α are fixed. It is clearly seen that the critical length n_c decreases from 11 to 4 as u increases from 1.0 to 2.0. The results indicate that a stronger e-e interaction u is advantageous for AFM order. This is reasonable since the on-site Hubbard repulsion is the origin of the AFM phase.

B. Confirmation by first-principles calculations

To check the correctness of our results, we have also performed first-principles calculations for polyacene. Geometries of the molecules are optimized using the QuantumATK package (ATK) [59,60] with a maximum residual force of 0.01 eV/Å. The spin-polarized generalized gradient approximation (SGGA) with Perdew-Burke-Ernzerhof (PBE) [61] parametrization is employed and a double-zeta plus single polarization (DZP) basis set is used for all atoms. Moreover, a mesh cutoff of 300 Rydberg is used for the real-space grid. The convergence criterion for the Hamiltonian is set to 1.0×10^{-4} Hartree in the electronic self-consistent-field loop. In Fig. 11(a), we present the relative total energy as a function of length for the NM, AFM, and FM spin states. The relative total energy demonstrates that the NM-AFM transition takes place at $n = 7$, which agrees well with our model calculations. The metastable FM state appears for $n = 9$, which is a little smaller than our model prediction of $n = 10$. The details of the spin density and the bond length around the critical length are presented in Fig. 11(b). The spin density shown in the insets of Fig. 11(b) displays the emergence of AFM order at $n = 7$. The bond length shows a solitonlike bond alternation at $n = 6$ and a uniform bond length in the middle of the molecule after the AFM state appears at $n = 7$. The change of bond lengths agrees with our calculation of lattice distortion in Fig. 6. We also examined the bond lengths around the critical length of the FM metastable spin state, where irregular bond

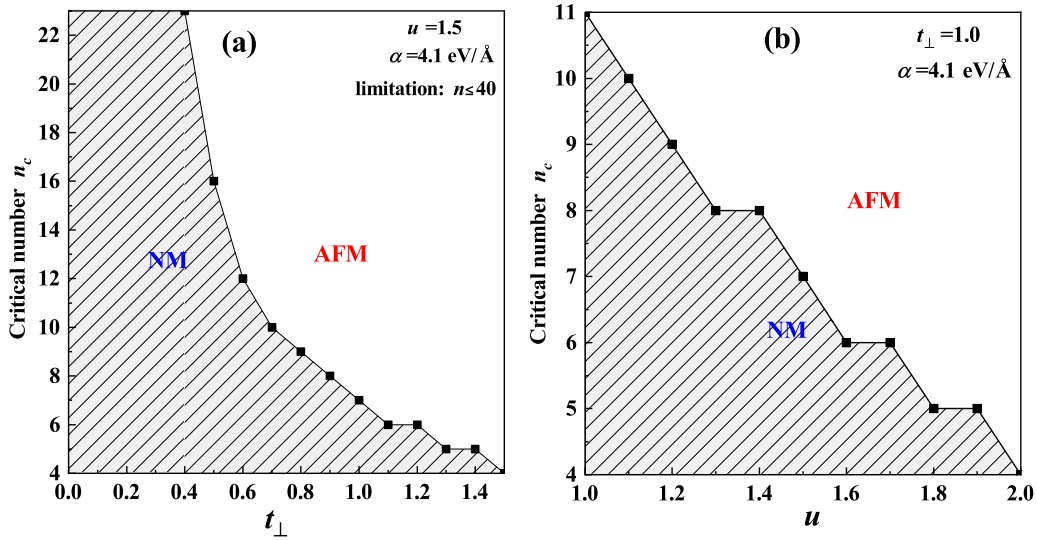

FIG. 10. Critical length n_c of the NM-AFM transition as a function of the value of (a) $t_\perp$ and (b) u.

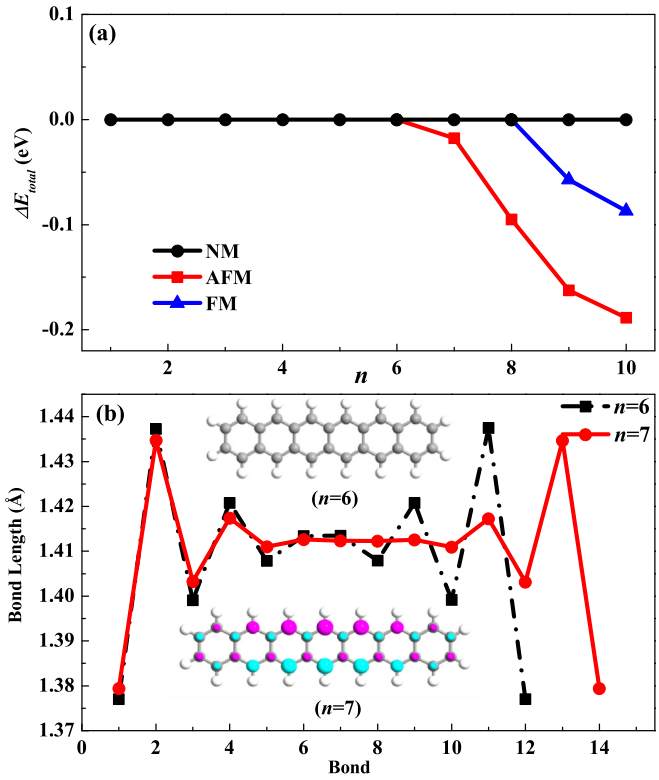

FIG. 11. (a) First-principles results for the relative total energy as a function of length for the NM, AFM, and FM states. (b) Spin density and bond lengths for $n = 6$ and 7. Insets: spin density for $n = 6$ and 7. The pink color denotes positive values and the blue color negative values.

distortions near the two ends of the molecule arise when the FM metastable spin state appears. By comparing with the results for the SSH model, we noted that the bond distortions for $n = 8$ in the middle of the molecule obtained from the first-principles calculation is a little smaller than for the SSH model, which results from the different algorithms for the intrinsic interactions and structural optimization. Hence, a smaller transition length of $n = 9$ is obtained in the ATK calculations due to the weaker suppression from the lattice. The present work focuses on the NM-AFM transition.

C. Extension to infinite chains

Although only finite polyacenes ($n \leqslant 12$) have been synthesized so far, here we would like to extend our analysis to infinite chains, which is expected to be useful for understanding the magnetism of other polymers with similar ladder structures. With the same parameters as in Fig. 2, we have checked for molecular lengths up to $n = 100$ that the lattice distortion along the chains is eliminated except for localized distortions near the two ends. The spin state of the system can thus be analyzed based on two coupled uniform chains. As shown above, without lattice distortion, the AFM state is favored, which is indeed what we find for long molecules. These results are consistent with other calculations for infinite polyacene chains [40,42]. The infinite polyacene chain can be viewed as a one-dimensional graphene nanoribbon with hydrogenation of the edges. The AFM edge states of graphene nanoribbons have been widely reported [62–64].

More generally, the present model gives hints for designing organic antiferromagnets by using two coupled polymer chains with similar ladder structure. Peierls distortion is detrimental to AFM order. If the tendency towards Peierls distortion is weak so that it is limited to the ends to the molecule, one should therefore use long molecules. Alternatively, one should ensure an odd number of sites per chain, even for short molecules or for strong Peierls distortion, since the resulting topological defect is advantageous to weaken the dimerization. Moreover, a stronger interchain coupling, stronger *e-e* interaction, and weaker *e-l* interaction are helpful to realize the AFM state.

IV. SUMMARY

In summary, we have investigated the electronic ground states in polyacene with an extended SSH model, where the *e-e* interaction, *e-l* interaction, and size effect are considered simultaneously. Our main focus was on the effects of lattice distortion and molecular size on the magnetism of finite molecules. A NM-AFM ground-state transition is found at a critical length of $n = 7$ rings. The mechanism of this length-dependent transition is explained in terms of the lattice distortion and the corresponding change of the average hopping rate of the π electrons. It is found that starting from the critical length, the lattice distortion in the middle of the molecule is strongly reduced, which leads to a decrease of the average hopping rate. The *e-e* interaction then stabilizes an antiferromagnetic spin density wave. In addition, the NM-AFM transition changes the length dependence of the molecular energy gap, which becomes weakly length dependent in the AFM state. We have also analyzed the effect of changing the strengths of interactions and hopping integrals on the NM-AFM transition, where larger *e-e* interaction and interchain hopping integral reduces the critical length. A larger *e-l* coupling suppresses the AFM state and increases the critical length. The results are confirmed by first-principles calculations. Finally, our results for hypothetical infinite polyacene supports these results, in particular the absence of dimerization away from the ends of the molecule and the stabilization of AFM order for long polyacenes. This work clarifies the mechanism of length-induced NM-AFM transition in polyacene and also provides suggestions for designing organic magnets with similar ladder structure.

ACKNOWLEDGMENTS

Support from the National Natural Science Foundation of China (Grants No. 11974215, No. 21933002, and No. 11874242) and the Natural Science Foundation of Shandong Province (Grant No. ZR2019MA043) are gratefully acknowledged. C.T. gratefully acknowledges support by the Deutsche Forschungsgemeinschaft via the Collaborative Research Center SFB 1143, project A04, and the Cluster of Excellence on Complexity and Topology in Quantum Matter ct.qmat (EXC 2147).

[1] J. W. Yoo, R. S. Edelstein, D. M. Lincoln, N. P. Raju, C. Xia, K. I. Pokhodnya, J. S. Miller, and A. J. Epstein, Phys. Rev. Lett. **97**, 247205 (2006).

[2] B. Li, M. Q. Zhou, Y. Lu, C. Y. Kao, J. W. Yoo, V. N. Prigodin, and A. J. Epstein, Org. Electron. **13**, 1261 (2012).

[3] G. C. Hu, Y. Guo, J. H. Wei, and S. J. Xie, Phys. Rev. B **75**, 165321 (2007).

[4] W. Z. Wang, Phys. Rev. B **73**, 235325 (2006).

[5] G. C. Hu, K. L. He, S. J. Xie, and A. Saxena, J. Chem. Phys. **129**, 234708 (2008).

[6] G. C. Hu, Z. Zhang, Y. Li, J. F. Ren, and C. K. Wang, Chin. Phys. B **25**, 057308 (2016).

[7] S. Pramanik, C. G. Stefania, S. Patibandla, S. Bandyopadhyay, K. Garre, N. Harth, and M. Cahay, Nat. Nanotechnol. **2**, 216 (2007).

[8] V. Dediu, M. Murgia, F. C. Matacotta, C. Taliani, and S. Barbanera, Solid. State Commun. **122**, 181 (2002).

[9] S. R. Chittipeddi, A. J. Epstein, J. H. Zhang, W. M. Reiff, I. Hamberg, D. B. Tanner, D. C. Johnson, and J. S. Miller, Synth. Met. **19**, 731 (1987).

[10] Z. Fang, Z. L. Liu, and K. L. Yao, Phys. Rev. B **49**, 3916 (1994).

[11] Z. Fang, Z. L. Liu, K. L. Yao, and Z. G. Li, Phys. Rev. B **51**, 1304 (1995).

[12] B. B. Jang, S. H. Lee, and Z. H. Kafafi, Chem. Mater. **18**, 449 (2006).

[13] M. A. Wolak, B. B. Jang, L. C. Palilis, and Z. H. Kafafi, J. Phys. Chem. B **108**, 5492 (2004).

[14] B. P. Rand, J. Genoe, P. Heremans, and J. Poortmans, J. Prog. Photovoltaics **15**, 659 (2007).

[15] M. Knupfer and H. Berger, Chem. Phys. **325**, 92 (2006).

[16] C. D. Lindstrom, M. Muntwiler, and X. Y. Zhu, J. Phys. Chem. B **111**, 6913 (2007).

[17] P. Stoliar, R. Kshirsagar, M. Massi, P. Annibale, C. Albonetti, D. M. de Leeuw, and F. J. Biscarini, Am. Chem. Soc. **129**, 6477 (2007).

[18] H. Iechi, Y. Watanabe, and K. Kudo, Jpn. J. Appl. Phys. **46**, 2645 (2007).

[19] F. Fujimori, K. Shigeto, T. Hamano, T. Minari, T. Miyadera, K. Tsukagoshi, and Y. Aoyagi, Appl. Phys. Lett. **90**, 193507 (2007).

[20] M. M. Payne, S. R. Parkin, and J. E. Anthony, J. Am. Chem. Soc. **127**, 8028 (2005).

[21] R. Mondal, B. K. Shah, and D. C. Neckers, J. Am. Chem. Soc. **128**, 9612 (2006).

[22] H. F. Bettinger, R. Mondal, and D. C. Neckers, Chem. Commun. **48**, 5209 (2007).

[23] D. Chun, Y. Cheng, and F. Wudl, Angew. Chem. Int. Ed. **47**, 8380 (2008).

[24] R. Mondal, C. Tönshoff, D. Khon, D. C. Neckers, and H. F. Bettinger, J. Am. Chem. Soc. **131**, 14281 (2009).

[25] C. Tönshoff and H. Bettinger, Angew. Chem. Int. Ed. **49**, 4125 (2010).

[26] I. Kaur, M. Jazdzyk, N. N. Stein, P. Prusevich, and G. P. Miller, J. Am. Chem. Soc. **132**, 1261 (2010).

[27] J. Krüger, F. García, F. Eisenhut, D. Skidin, J. M. Alonso, E. Guitián, D. Pérez, G. Cuniberti, F. Moresco, and D. Peña, Angew. Chem. Int. Ed. **56**, 11945 (2017).

[28] J. Krüger, F. Eisenhut, D. Skidin, T. Lehmann, D. A. Ryndyk, G. Cuniberti, F. García, J. M. Alonso, E. Guitián, D. Pérez, D. Peña, G. Trinquier, J. P. Malrieu, F. Moresco, and C. Joachim, ACS Nano **12**, 8506 (2018).

[29] R. Zuzak, R. Dorel, M. Kolmer, M. Szymonski, S. Godlewski, and A. M. Echavarren, Angew. Chem. Int. Ed. **57**, 10500 (2018).

[30] B. Shen, J. Tatchen, E. S. Garcia, and H. F. Bettinger, Angew. Chem. **130**, 10666 (2018).

[31] F. Eisenhut, T. Kühne, F. García, S. Fernandez, E. Guitian, D. Perez, G. Trinquier, G. Cuniberti, C. Joachim, D. Peña, and F. Moresco, ACS Nano **14**, 1011 (2020).

[32] R. Pilevarshahri, I. Rungger, T. Archer, S. Sanvito, and N. Shahtahmassebi, Phys. Rev. B **84**, 174437 (2011).

[33] S. Berkebile, P. Puschnig, G. Koller, M. Oehzelt, F. P. Netzer, C. Ambrosch-Draxl, and M. G. Ramsey, Phys. Rev. B **77**, 115312 (2008).

[34] M. Bendikov, H. M. Duong, K. Starkey, K. N. Houk, E. A. Carter, and F. Wudl, J. Am. Chem. Soc. **126**, 7416 (2004).

[35] D. E. Jiang and S. Dai, J. Phys. Chem. A **112**, 332 (2008).

[36] M. C. dos Santos, Phys. Rev. B **74**, 045426 (2006).

[37] H. Angliker, E. Rommel, and J. Wirz, Chem. Phys. Lett. **87**, 208 (1982).

[38] K. N. Houk, P. S. Lee, and M. Nendel, J. Org. Chem. **66**, 5517 (2001).

[39] J. Hachmann, J. J. Dorando, M. Avilés, and G. K. L. Chan, J. Chem. Phys. **127**, 134309 (2007).

[40] Z. X. Qu, D. W. Zhang, C. G. Liu, and Y. S. Jiang, J. Phys. Chem. A **113**, 7909 (2009).

[41] S. Kivelson and O. L. Chapman, Phys. Rev. B **28**, 7236 (1983).

[42] M. P. O'Connor and R. J. Watts-Tobin, J. Phys. C: Solid State Phys. **21**, 825 (1988).

[43] J. S. Qi, Y. Y. Miao, Y. J. Cui, S. Qiu, J. M. Zhao, G. P. Zhang, J. F. Ren, C. K. Wang, and G. C. Hu, Results Phys. **27**, 104510 (2021).

[44] A. Aadhityan, C. P. Kala, and D. J. Thiruvadigal, Appl. Surf. Sci. **418**, 393 (2017).

[45] D. Q. Zou, B. Cui, X. R. Kong, W. K. Zhao, J. F. Zhao, and D. S. Liu, Phys. Chem. Chem. Phys **17**, 11292 (2015).

[46] S. Caliskan and A. Laref, Sci. Rep. **4**, 7363 (2014).

[47] W. P. Su, J. R. Schrieffer, and A. J. Heeger, Phys. Rev. Lett. **42**, 1698 (1979).

[48] H. Jiang, X. N. Hu, Y. C. Zhao, and C. Zhang, J. Electron. Mater. **46**, 1005 (2017).

[49] Z. J. Li, H. Q. Lin, Z. An, and K. L. Yao, J. Chem. Phys **109**, 10082 (1998).

[50] H. Jiang, G. C. Hu, and S. J. Xie, Phys. B (Amsterdam, Neth.) **405**, S299 (2010).

[51] C. Tönshoff and H. F. Bettinger, Chem. Eur. J. **27**, 3193 (2021).

[52] A. Pomogaeva, M. Filatov, and C. H. Choi, Carbon Trends **7**, 100146 (2022).

[53] Z. Fang, Z. L. Liu, K. L. Yao, and H. F. Hu, Commun. Theor. Phys. **28**, 29 (1997).

[54] L. Zhao and Z. L. Wang, J. China Three Gorges Univ. **26**, 2 (2004).

[55] A. W. Overhauser, Phys. Rev. **128**, 1437 (1962).

[56] N. Majlis, *The Quantum Theory of Magnetism* (World Scientific, Singapore, 2000).

[57] J. A. Blackman and M. K. Sabra, Phys. Rev. B **47**, 15437 (1993).

[58] W. Z. Wang, Z. L. Liu, and K. L. Yao, Phys. Rev. B **55**, 12989 (1997).
[59] J. M. Soler, E. Artacho, J. D. Gale, A. García, J. Junquera, P. Ordejón, and D. Sánchez-Portal, J. Phys.: Condens. Matter **14**, 2745 (2002).
[60] Atomistix ToolKit version 2018.06, Synopsys QuantumWise A/S, www.quantumwise.com.
[61] J. P. Perdew, K. Burke, and M. Ernzerhof, Phys. Rev. Lett. **77**, 3865 (1996).
[62] M. Kan, J. Zhou, Q. Sun, Q. Wang, Y. Kawazoe, and P. Jena, Phys. Rev. B **85**, 155450 (2012).
[63] X. Q. Lin and J. Ni, Phys. Rev. B **84**, 075461 (2011).
[64] C. Cocchi, D. Prezzi, A. Calzolari, and E. Molinari, J. Chem. Phys. **133**, 124703 (2010).